

A simplified model of the source channel of the Leksell GammaKnife[®] tested with PENELOPE 1

Feras M.O. Al-Dweri and Antonio M. Lallena

Departamento de Física Moderna, Universidad de Granada, E-18071 Granada, Spain.

Manuel Vilches

Servicio de Radiofísica, Hospital Clínico “San Cecilio”, Avda. Dr. Olóriz, 16, E-18012 Granada, Spain.

Monte Carlo simulations using the code PENELOPE have been performed to test a simplified model of the source channel geometry of the Leksell GammaKnife[®]. The characteristics of the radiation passing through the treatment helmets are analysed in detail. We have found that only primary particles emitted from the source with polar angles smaller than 3° with respect to the beam axis are relevant for the dosimetry of the Gamma Knife. The photons trajectories reaching the output helmet collimators at $(x, y, z = 236 \text{ mm})$, show strong correlations between $\rho = (x^2 + y^2)^{1/2}$ and their polar angle θ , on one side, and between $\tan^{-1}(y/x)$ and their azimuthal angle ϕ , on the other. This enables us to propose a simplified model which treats the full source channel as a mathematical collimator. This simplified model produces doses in excellent agreement with those found for the full geometry. In the region of maximal dose, the relative differences between both calculations are within 3%, for the 18 and 14 mm helmets, and 10%, for the 8 and 4 mm ones. Besides, the simplified model permits a strong reduction (larger than a factor 15) in the computational time.

1. Introduction

Leksell GammaKnife[®] (GK) is an instrument that permits a precise external irradiation to treat intracranial lesions. Concentrating the radiation coming from 201 ⁶⁰Co sources, a high dose can be delivered to the target area with an accuracy better than 0.3 mm (Wu *et al* 1990, Elekta 1992, Benjamin *et al* 1997). Besides, the sharp dose gradient allows to reduce the doses absorbed by the critical brain structures surrounding the lesion to be treated. The size and shape of the final beam can be fixed by combining different treatment helmets with an adequate configuration of plugged and unplugged sources. In this way the isodose distribution curves can be modified in the optimal way. The GK is used together with GammaPlan[®] (GP), a planning system which uses semi-empirical algorithms with various approximations to calculate the doses, and assumes that the target is composed of unit density material (Wu *et al* 1990, Wu 1992, Elekta 1996).

To ensure the quality of the planning system, an experimental verification is needed (Hartmann *et al* 1995), but the difficulties inherent to the physical dose measurements make Monte Carlo (MC) simulations to be a good complementary tool to achieve this purpose. In the case of the GK, a number of such calculations have been performed in the last few years. Most of them have been done with EGS4 (Cheung *et al* 1998, 1999a, 1999b, 2000, Xiaowei and Chunxiang 1999) and have shown no relevant differences from GP calculations for a homogeneous phantom. However, in stereotactic radiosurgery, Solberg *et al* (1998) have pointed out a remarkable disagreement between MC results and those predicted by the usual planning systems, once phantom inhomogeneities are taken into account. For the GK, Cheung *et al* (2001) have found discrepancies up to 25% in case of extreme conditions (mainly near tissue interfaces and dose edges.)

Recently, Moskvin *et al* (2002) have performed a detailed study in which they have determined the characteristics of the beams emitted after the helmets and have used them to

calculate the dose field inside a polystyrene phantom. These authors have used PENELOPE (v. 2000) and have found a good agreement with the calculations performed in previous works and with the predictions of the GP, what ensures the suitability of PENELOPE for this kind of simulations.

In the present work we want to go deeper in some of the basic aspects analysed by Moskvina and collaborators (2002). We have simulated a single source of the GK using the version 2001 of PENELOPE (Salvat *et al* 2001) and we have investigated the energy spectra, the particle spatial distributions and the correlations between the polar and azimuthal angles of the particle trajectories and the coordinates of the point these trajectories reach the treatment helmets. The results we have obtained permit a simplification of the full geometry which allows a considerable reduction of the simulation CPU time, without loss of accuracy in the doses delivered to the phantom.

In the next section we describe the geometrical model we have used to simulate the single source of the GK as well as the relevant details concerning the MC calculations we have performed. Section 3 is devoted to discuss the results we have obtained and study the geometrical simplification we propose. Finally we draw our conclusions.

2. Material and Methods

2.1. Leksell GammaKnife[®] model

Details concerning the GK geometry have been obtained from the User Manual (Elekta 1992). In actual simulations, the different pieces forming the head and the collimating system have been described by the specific geometries sketched in figure 1.

Figure 1a shows the capsule. It is made of stainless steel (SS) and includes the ⁶⁰Co active core. The latter (in black in the figure) is formed by 20 cylindrical pellets of 1 mm diameter and 1 mm height. In our simulations, the active core is considered as an unique cylindrical source of 1 mm diameter and 20 mm height made of cobalt.

The capsule is inside a bushing system made of aluminum. In our simulations we have used the simplified geometry plotted in figure 1b.

Figure 1c shows the geometry we have considered for the collimation system of the single source. The radiation coming from the ⁶⁰Co source is collimated by a stationary collimator (located in the central body) and an additional collimator located in the helmet. The first one is made of tungsten and lead, while that of the helmet is of tungsten. Four different helmets are available, producing beams with nominal aperture diameters of 4, 8, 14 and 18 mm at the focal point of the system, which is located at 401 mm from the source centre. The inner and outer collimator diameters of the helmets we have used are given in table 1 and have been taken from Moskvina *et al* (2002).

Finally, figure 1d shows the complete geometry including the head of the instrument (which is made of iron) and the phantom used to simulate the patient head. The latter is a sphere of 160 mm of diameter, filled with water and centered in the focus. The situation of the single source channel we have considered in our simulations is also shown.

2.2. Monte Carlo calculations

In this work we have used the PENELOPE (v. 2001) MC code (Salvat *et al* 2001) to perform the simulations. PENELOPE is a general purpose MC code which allows to simulate the coupled electron-photon transport. It can be applied for energies ranging from a few hundred

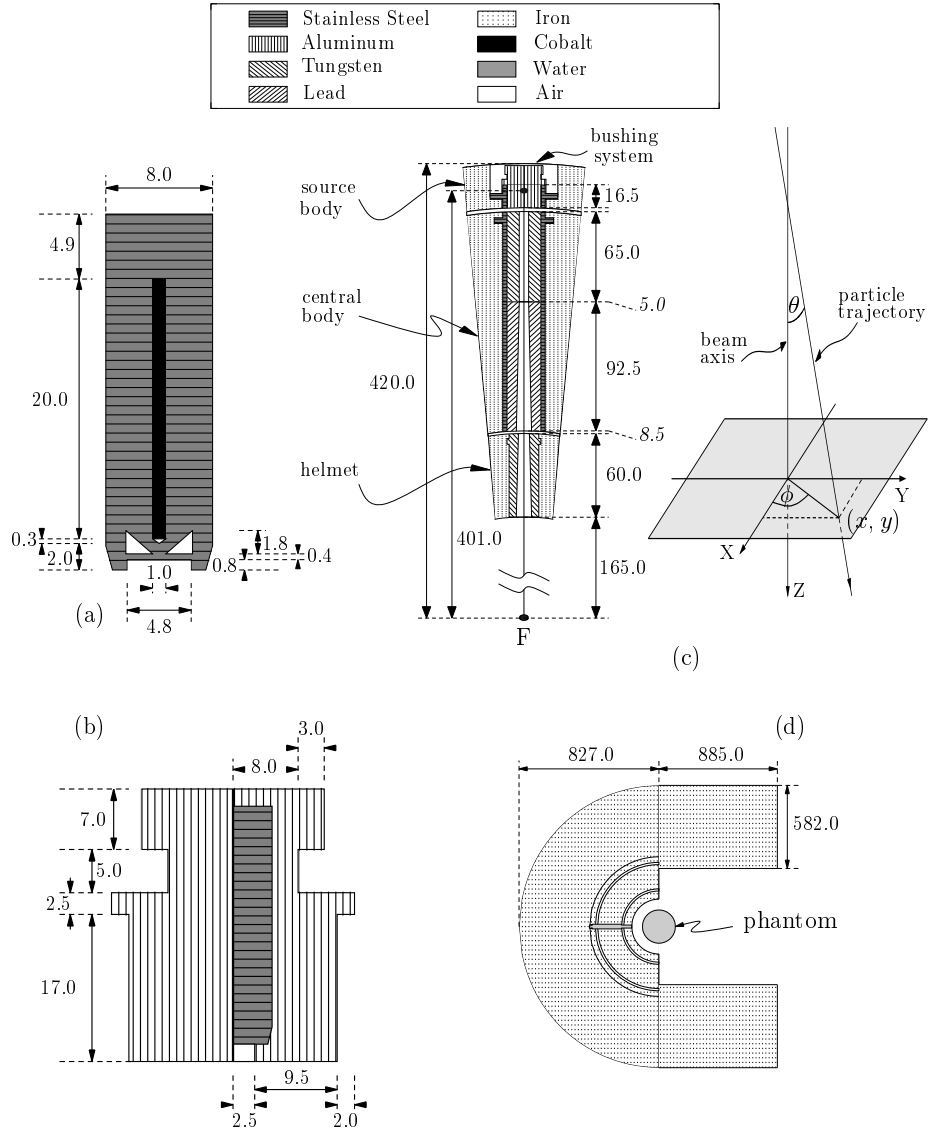


Figure 1. Schematic view of the geometrical models used in our simulations for the different parts of the GK: (a) capsule involving the radionuclide; (b) bushing system surrounding the capsule; (c) full collimation system for a single source, and (d) head of the GK showing the situation of the water phantom. Distances are in mm. The values in italic give the collimator apertures at the corresponding positions. F labels the focus of the collimation system. In panel (c) the scheme showing the polar and azimuthal angles and the (x, y) coordinates along the beam line is also included.

eV up to 1 GeV, for electrons, photons and positrons and for arbitrary materials. Besides, PENELOPE permits a good description of the particle transport at the interfaces and presents an accurate simulation at low energies. As an example we mention here that the code has been used to simulate an accelerator head, obtaining results in good agreement with measurements (Sempau *et al* 2001).

In PENELOPE, analog simulation is performed for photons. On the other hand, electron and positron simulation is done in a mixed scheme in which collisions are classified in two

Table 1. Inner and outer helmet collimator apertures of the Leksell GammaKnife[®]. The values have been taken from Moskvin *et al* (2002).

| Final beam diameter | 4 mm | 8 mm | 14 mm | 18 mm |
|---------------------------------------|------|------|-------|-------|
| Inner helmet collimator aperture [mm] | 2.0 | 3.8 | 6.3 | 8.3 |
| Outer helmet collimator aperture [mm] | 2.5 | 5.0 | 8.5 | 10.6 |

types: hard and soft. Hard collisions are simulated in a detailed way and are characterised by polar angular deflections or energy losses larger than certain cutoff values. Soft collisions do not fulfil these conditions and their effects are described in terms of a condensed simulation based on a multiple scattering theory. The electron tracking is controlled by means of four parameters: C_1 and C_2 , W_{cc} and W_{cr} . The first two refer to elastic collisions. C_1 gives the average angular deflection produced by multiple elastic scattering along a path length equal to the mean free path between consecutive hard elastic events. C_2 represents the maximum value permitted for the average fractional energy loss between consecutive hard elastic events. On the other hand, W_{cc} and W_{cr} are energy cutoffs to separate hard and soft events. Thus, the inelastic electron collisions with energy loss $W < W_{cc}$ and the emission of Bremsstrahlung photons with energy $W < W_{cr}$ are considered in the simulation as soft interactions. The particles are simulated for energies above a given absorption energy, E_{abs} , below which they are absorbed locally. Besides, the length of the steps generated in the simulation is limited by an upper bound, s_{max} . Table 2 shows the values of these parameters for the various materials used in our simulations. The values fixed for the different parameters in the various materials permit to obtain results in reasonable CPU times. The key point here concerns the relative large absorption energies adopted for electrons in the heavier materials, where high energy electrons produce a very large number of secondary particles. These particles are not relevant for the dosimetry in the phantom and the E_{abs} value we have chosen avoid the loss of CPU time following their tracks. We have checked that the use of the parameter set shown in table 2 does not affect the precision of the final results.

To finish with the description of the MC code, it is worth to mention the main differences between the version 2001 that we have used and the 2000, used by Moskvin *et al* (2002), of PENELOPE. These affect the model used to describe the electron and positron elastic collisions, the Bremsstrahlung emission produced by electrons and positrons, the photon photoelectric absorption cross sections and the fluorescence processes taken into account. Details can be found in Salvat *et al* (2001). We have performed some basic simulations using both versions of the code and the results obtained showed no differences. Then we do not expect differences between our results and those of Moskvin *et al* (2002) other than those linked to possible differences in the geometries considered.

The radionuclide was assumed to be uniformly distributed inside the active core. ^{60}Co decays via β^- to excited ^{60}Ni . However, the emitted electrons do not exit the bushing assembly. Excited ^{60}Ni decays to its ground state by emitting two photons with energies 1.17 and 1.33 MeV. In our simulations we have assumed that photons are emitted with the average energy 1.25 MeV. This does not produce any effect on the results. The direction of the emitted photons was supposed to be isotropic around the initial position. In actual calculations, and in order to perform the simulations in reasonable times, this direction was

Table 2. Tracking parameters of various materials assumed in our PENELOPE simulations. $E_{\text{abs}}(\gamma)$ and $E_{\text{abs}}(e^-, e^+)$ stand for the absorption energies corresponding to photons and electrons and positrons, respectively.

| | materials | | |
|----------------------------------|-----------|-------------------|-----------|
| | Air | Water, SS, Al, Co | Fe, Pb, W |
| $E_{\text{abs}}(\gamma)$ [keV] | 1.0 | 1.0 | 1.0 |
| $E_{\text{abs}}(e^-, e^+)$ [keV] | 0.1 | 50.0 | 500.0 |
| C_1 | 0.05 | 0.1 | 0.1 |
| C_2 | 0.05 | 0.05 | 0.05 |
| W_{cc} [keV] | 5.0 | 5.0 | 5.0 |
| W_{cr} [keV] | 1.0 | 1.0 | 1.0 |
| s_{max} [cm] | 10^{35} | 10^{35} | 10^{35} |

sampled in a cone with a given semi-aperture θ_{max} . Then, $w = \cos \theta_i$, with θ_i the initial polar angle of the direction of the emitted photons, was sampled uniformly between 1 and $\cos \theta_{\text{max}}$ and the initial azimuthal angle ϕ_i was sampled uniformly between 0 and 2π .

The statistical uncertainties were calculated by scoring, in each voxel, both the quantity of interest Q and its square for each history. Thus, the MC estimate of the quantity is given by

$$Q_{\text{mean}} = \frac{1}{N} \sum_{i=1}^N q_i,$$

where N is the number of simulated histories and q_i is the value scored by all particles of the i -th history (that is, including the primary particle and all the secondaries it generates). The statistical uncertainty is given by

$$\sigma_{Q_{\text{mean}}} = \sqrt{\frac{1}{N} \left[\frac{1}{N} \sum_{i=1}^N q_i^2 - Q_{\text{mean}}^2 \right]}.$$

If the contributions q_i take the values 0 and 1 only, the standard error can be evaluated as

$$\sigma_{Q_{\text{mean}}} = \sqrt{\frac{1}{N} Q_{\text{mean}} (1 - Q_{\text{mean}})}.$$

The number of histories simulated has been chosen in each case to maintain these statistical uncertainties under reasonable levels. The uncertainties given throughout the paper correspond to 1σ .

The geometries discussed in the previous section were described by means of the geometrical package PENGEOM of PENELOPE in terms of quadric surfaces. Table 3 gives the composition and densities of the different materials used in our simulations.

The system for a single source presents cylindrical symmetry. The reference system was located with the origin in the centre of the active core, with the z axis along the source and pointing toward the phantom. The different magnitudes, and in particular the dose rate $D(\rho, z)$, were supposed to be functions of the z and $\rho = (x^2 + y^2)^{1/2}$ coordinates.

Table 3. Composition (in weight fraction) and densities of various materials assumed in our PENELOPE simulations.

| | Compound Materials | | | Elementary Materials | | | | |
|-------------------------------|--------------------|---------|----------|----------------------|--------|-------|-------|----------|
| | Air | SS | Water | Aluminum | Cobalt | Iron | Lead | Tungsten |
| H | | | 0.111894 | | | | | |
| C | 0.000124 | 0.00026 | | | | | | |
| N | 0.755267 | | | | | | | |
| O | 0.231781 | | 0.888106 | | | | | |
| Al | | | | 1.0 | | | | |
| Si | | 0.0042 | | | | | | |
| P | | 0.00019 | | | | | | |
| S | | 0.00003 | | | | | | |
| Ar | 0.012827 | | | | | | | |
| Cr | | 0.1681 | | | | | | |
| Mn | | 0.014 | | | | | | |
| Fe | | 0.6821 | | | | 1.0 | | |
| Co | | | | | 1.0 | | | |
| Ni | | 0.1101 | | | | | | |
| Mo | | 0.0211 | | | | | | |
| W | | | | | | | | 1.0 |
| Pb | | | | | | | 1.0 | |
| density [g cm ⁻³] | 0.0012048 | 7.8 | 1.0 | 2.6989 | 8.9 | 7.874 | 11.35 | 19.3 |

The full volume of the water phantom was subdivided into annular volume bins with thicknesses $\Delta\rho = 0.5$ mm and $\Delta z = 1$ mm in case of the 18 and 14 mm treatment helmets. For the smaller ones, 8 and 4 mm, the values considered were $\Delta\rho = 0.25$ mm and $\Delta z = 0.5$ mm

3. Results

3.1. Effective emission angle

The first point to be fixed in order to perform the simulations is to determine the value of the semi-aperture θ_{\max} of the cone where the direction of the initial photon is sampled. To do that we have defined the “effective emission angle”, $\theta_{\text{eff}}^\alpha$, as the angle θ_i of the direction of an emitted primary photon such as it, or any of the secondary particles it creates passing through the collimator, reaches a certain region α (e.g. a body or a plane) in the simulation geometry. In particular we have studied the distribution of the effective emission angle at the water phantom, $\theta_{\text{eff}}^{\text{phantom}}$.

Moskvin *et al* (2002) sampled the initial directions of the emitted photons in a cone with 10° of semi-aperture and checked that no differences, within statistical uncertainties, were observed by increasing this value up to 90° for the 18 mm helmet. We have performed a simulation with the full geometry of the GK, for the 18 mm helmet. A total of $6 \cdot 10^7$ histories were followed and the initial directions were sampled in a cone with semi-aperture $\theta_{\max} = 20^\circ$. The distribution of the fraction of initial photons vs. the cosine of $\theta_{\text{eff}}^{\text{phantom}}$ is shown in figure 2. As we can see, the distribution reduces by three orders of magnitude between 0° and 5° . The insert in the same figure shows, with more detail, the distribution in this interval. The number of counts for $\theta_{\text{eff}}^{\text{phantom}} = 2^\circ$ (3°) is more than two (three) orders of magnitude smaller than for $\theta_{\text{eff}}^{\text{phantom}} \sim 0^\circ$.

Despite that a semi-aperture of 3° for the cone in which the initial directions are sampled is considerably smaller than that used by Moskvin *et al* (2002), we have checked that it

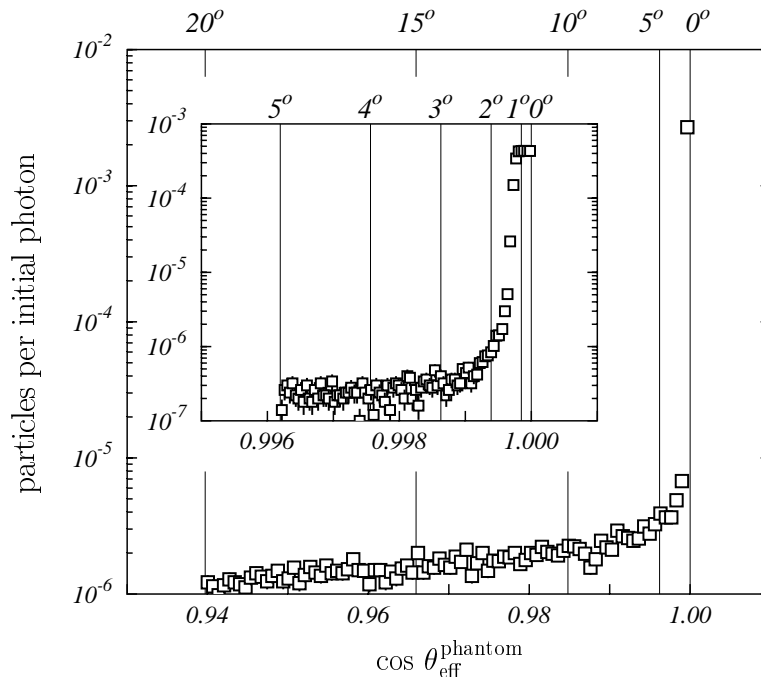


Figure 2. Distribution of particles per initial photon vs. the cosine of the effective emission angle at the water phantom, in the case of the 18 mm helmet. A maximum emission angle $\theta_{\max} = 20^\circ$ has been used in the simulations.

suffices to obtain right doses in the phantom. We have performed a simulation in the previous conditions, following $15 \cdot 10^7$ histories. The dose $D(\rho, z_0)$ per disintegration in planes transverse to the beam axis direction with $z_0 = 350, 401$ and 450 mm (these are before the focus, at the focus and after it, respectively) are plotted in figure 3, as a function of the distance to the beam axis, ρ . Therein black squares stand for the full calculation (that is sampling the initial directions into the cone with semi-aperture 20°), while open circles give the dose due to histories whose the primary particle was emitted with an angle $\theta_i \leq 3^\circ$. Both linear (left) and logarithmic (right) plots are included to see the small and large ρ behaviour clearly. As we can see both results coincide within the statistical uncertainties and, as a consequence, we can state that a maximum polar angle $\theta_{\max} = 3^\circ$ for sampling the initial particle direction is enough to ensure the accuracy of the results.

3.2. Comparison with previous results

With the value $\theta_{\max} = 3^\circ$ determined as explained in the previous section, we have performed simulations considering the full geometry of the GK and following $6 \cdot 10^7$ histories.

Figure 4 shows the dose profiles in the plane of the focus, transverse to the beam axis ($z = 401$ mm) for the four helmets. Therein the squares correspond to the simulations we have performed, normalised to the maximum. Full curves show the results of Cheung *et al.* (1998), while broken curves are given by the manufacturer.‡ The agreement with the results of Cheung *et al.* (1998) is very good (these authors quoted an error below 1% at dose

‡ These two sets of results have been obtained by scanning directly figures 1-4 of Cheung *et al.* (1998).

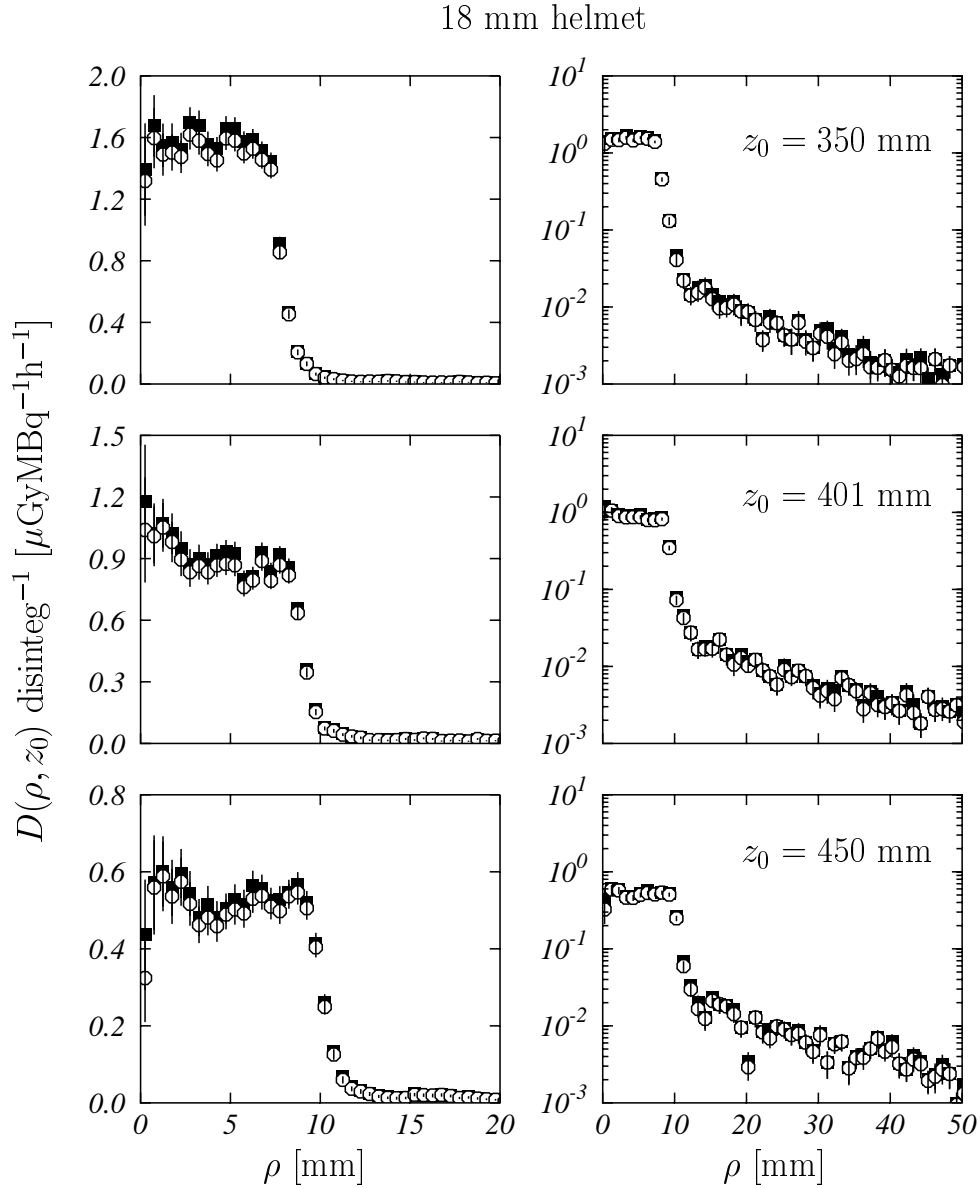


Figure 3. Dose profiles (per disintegration) for the 18 mm helmet as a function of the radial distance from the beam axis ρ . The results obtained at the planes $z_0 = 350$, 401 and 450 mm are shown. The simulations have been performed for $\theta_{\max} = 20^\circ$. Black squares correspond to the dose deposited in all the histories followed, while open circles show the dose deposited in those histories in which the primary photons were emitted with $\theta_i \leq 3^\circ$ only. Left (right) panels are in linear (semi-logarithmic) scale. The values include the geometrical factor $(1 - \cos 20^\circ)/2$ which renormalizes the number of particles emitted in the 20° cone to the total number of particles emitted in actual situations (which correspond to polar angles between 0 and π).

maximum), while a clear discrepancy with data provided by the manufacturer appears in the tail of the distributions.

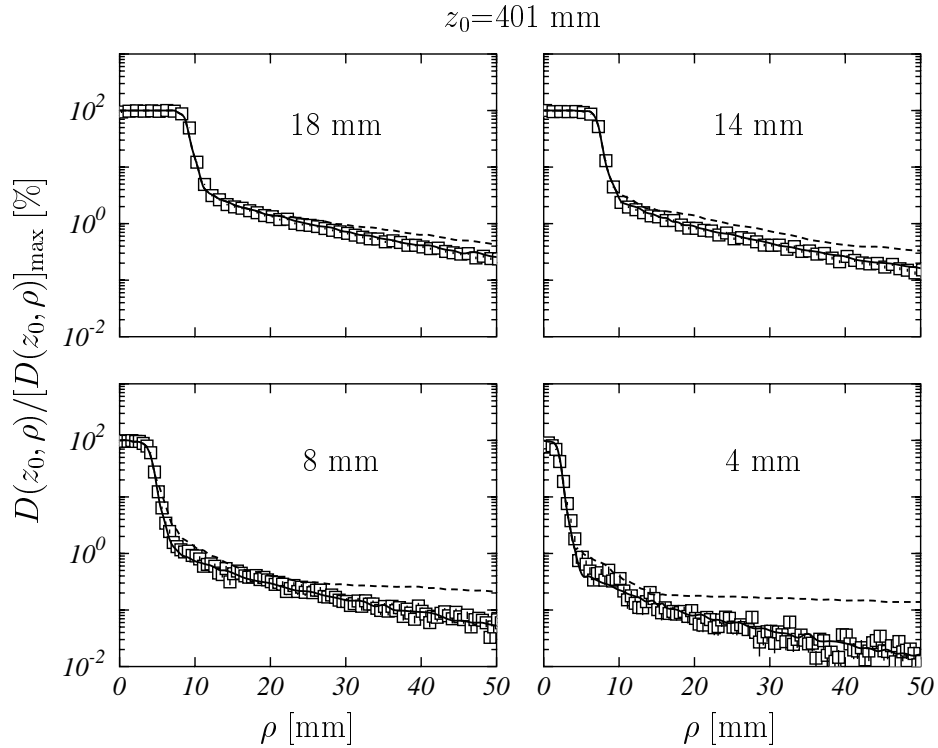


Figure 4. Dose profiles (relative to their maximum) as a function of the radial distance from the beam axis ρ . The results obtained in our simulations at the plane $z_0 = 401$ mm for the four helmets (open squares) are compared with the results of Cheung *et al* (1998) (solid lines) and with the data provided by the manufacturer (broken curves).

Table 4 quotes the values we have obtained for the ρ distance providing 50% of the maximum dose, ρ_{50} , and the penumbra, determined as the difference $\rho_{80} - \rho_{20}$ between the distances providing 80 and 20% of the maximum dose. In this table our findings are compared

Table 4. Values of ρ_{50} and penumbra ($\rho_{80} - \rho_{20}$) obtained for the four helmets and compared with the results quoted in Wu *et al* (1990). ρ_{80} , ρ_{50} and ρ_{20} stand for the ρ distances providing, respectively, the 80, 50 and 20% of the maximum dose in the plane of the focus, transverse to the beam axis ($z = 401$ mm).

| | This work | | Wu <i>et al</i> (1990) | |
|-------|------------------|------------------------------|------------------------|------------------------------|
| | ρ_{50} [mm] | $\rho_{20} - \rho_{80}$ [mm] | ρ_{50} [mm] | $\rho_{20} - \rho_{80}$ [mm] |
| 4 mm | 2.0 ± 0.3 | 1.1 ± 0.4 | 2.0 | 1-2 |
| 8 mm | 4.2 ± 0.3 | 1.4 ± 0.4 | 4.2 | |
| 14 mm | 7.2 ± 0.5 | 1.4 ± 0.7 | 7.0 | |
| 18 mm | 9.1 ± 0.5 | 1.3 ± 0.7 | 9.0 | |

with those of Wu *et al* (1990) and, as we can see, the agreement is excellent.

3.3. Characteristics of the beam after the helmets

Now we analyse the characteristics of the beam after it goes through the outer collimators of the helmets. We have performed simulations with the full geometry of the GK, sampling the initial directions with $\theta_{\max} = 3^\circ$ and following $6 \cdot 10^7$ histories.

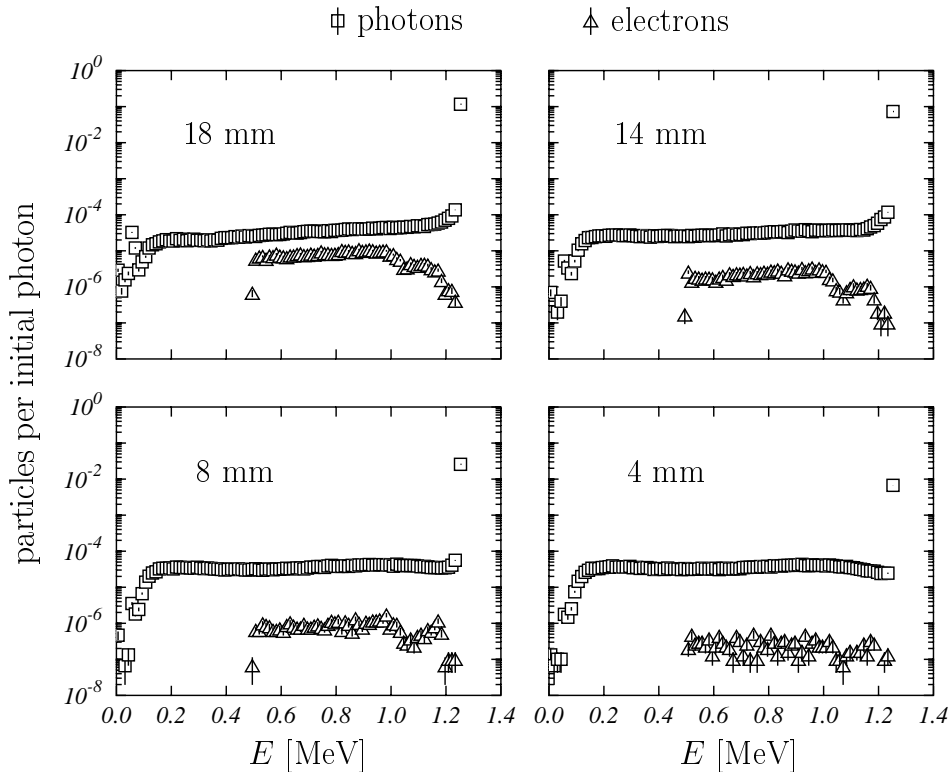


Figure 5. Distributions of particles per initial photon vs. the energy at the output collimators of the four treatment helmets. Squares (triangles) correspond to photons (electrons).

First we have studied the energy spectra at the output collimators of the four helmets and for both photons (squares) and electrons (triangles). Results are plotted in figure 5. In the four cases, the photon spectra show a pronounced peak corresponding to the initial energy. For lower energies, the spectra are rather uniform. Below 100 keV, the peaks due to characteristic x rays emitted after the relaxation of vacancies produced in K shells of the tungsten or lead atoms of the collimation system can be distinguished, especially for the 18 mm helmet. In general the number of particles exiting the output collimators of the helmets diminishes, as expected, with their aperture.

In what respect to electrons, one can see that their relative importance reduces with the aperture of the helmet. On the other hand, the artificial discontinuity at 500 keV is due to the corresponding absorption energy in the materials forming the collimators.

In view of these results, we can say that most of the particles traversing the helmet output collimators have the initial energy and, as a consequence, they are primary photons

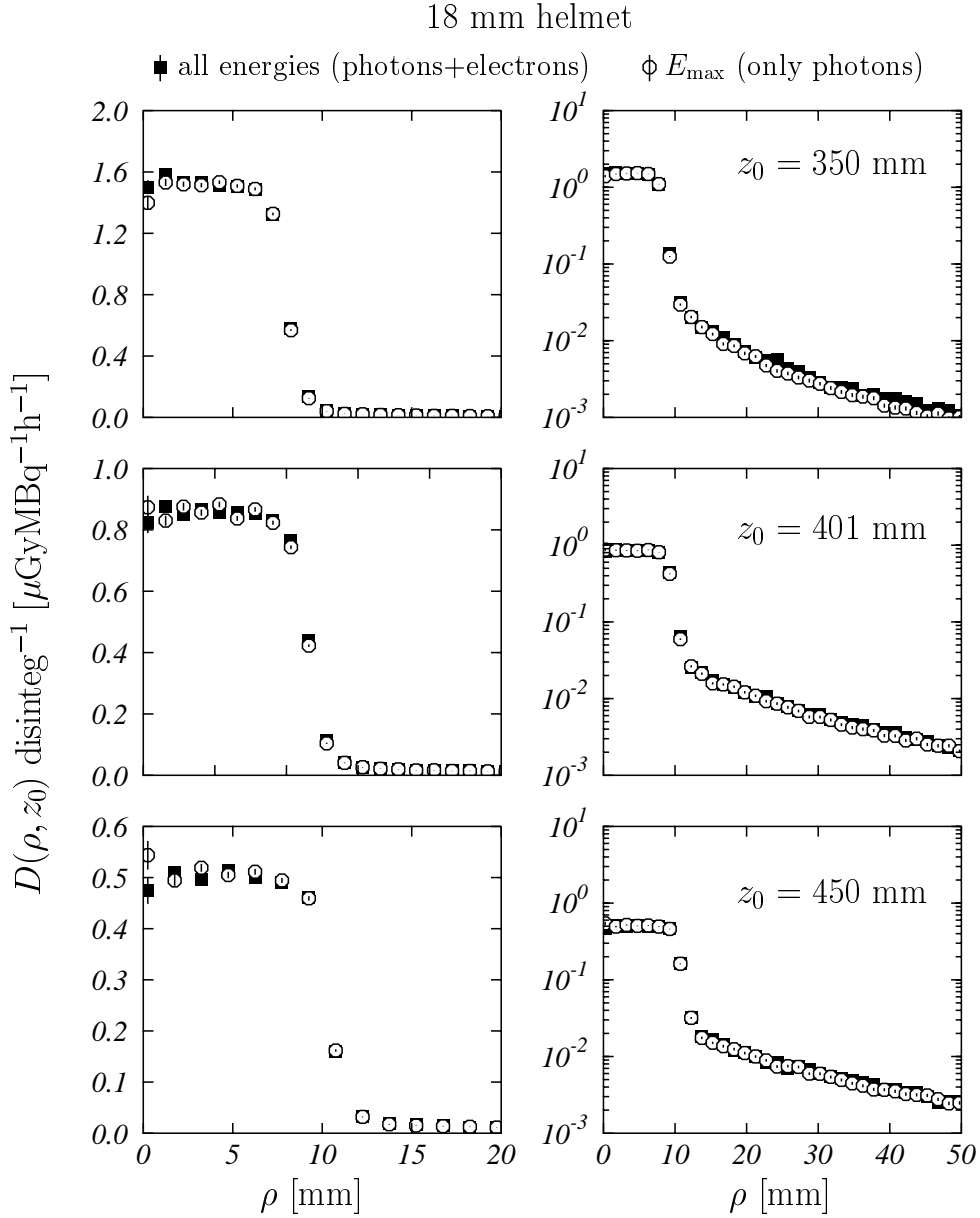


Figure 6. Dose profiles (per disintegration) for the 18 mm helmet as a function of the radial distance from the beam axis ρ . The results obtained at the planes $z_0 = 350$, 401 and 450 mm are shown. The simulations have been performed for $\theta_{\max} = 3^\circ$. Black squares correspond to the dose deposited by photons and electrons with any energy, while open circles give the dose due to photons with the maximum energy only. Left (right) panels are in linear (semi-logarithmic) scale. The values include the geometrical factor $(1 - \cos 3^\circ)/2$ which renormalizes the number of particles emitted in the 3° cone to the total number of particles emitted in actual situations (which correspond to polar angles between 0 and π).

coming directly from the source or, at most, having suffered a Rayleigh (elastic) scattering. In figure 6 we test the extent to which the previous statement is correct for the 18 mm helmet.

Therein we have plotted the dose $D(\rho, z_0)$ per disintegration in the planes $z_0 = 350, 401$ and 450 mm, as a function of the distance ρ to the beam axis. Left panels correspond to linear plots, while the right ones are logarithmic plots pointing out the situation for large ρ values. Black squares correspond to the full simulation, whereas open circles are the results obtained by taking into account the photons arriving to the phantom with the initial energy, only. As we can see, the differences between both results are rather small.

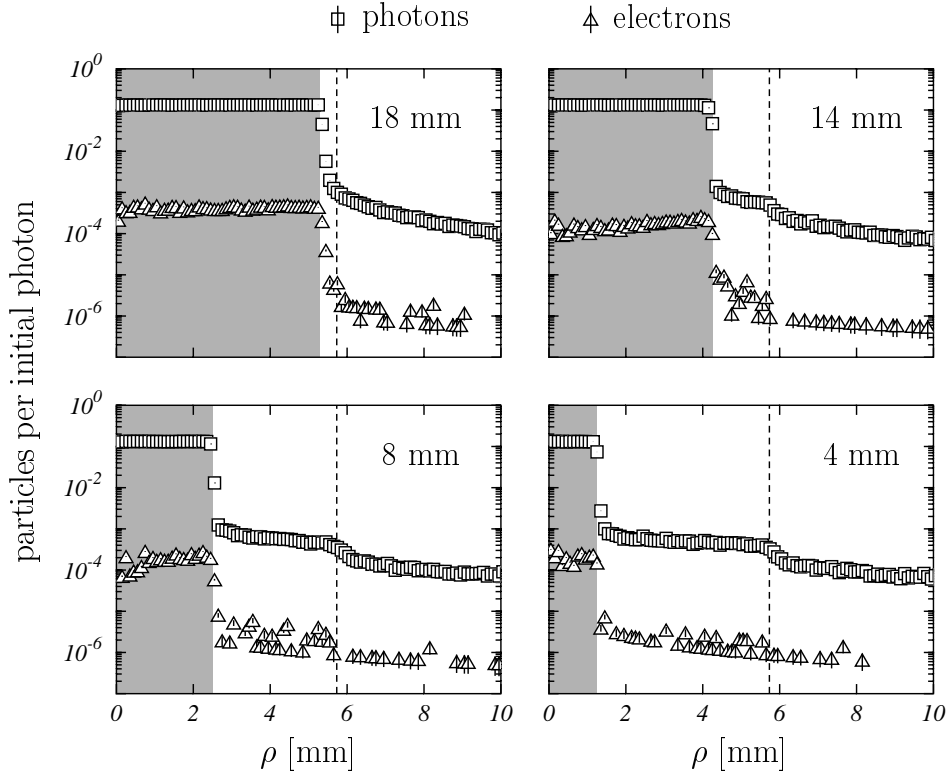


Figure 7. Distributions of particles per initial photon vs. the radial distance from the beam axis ρ at the output collimators of the four treatment helmets. Shadow regions represent the semi-aperture of these collimators. Squares (triangles) correspond to photons (electrons). The dashed line indicates the semi-aperture of the beam at the same z , if the helmets were not present.

The second point of interest concerns the particle spatial distribution at the helmet output collimators. Figure 7 shows the particle distributions in the transverse direction ρ for the four treatment helmets. Squares (triangles) correspond to photons (electrons). The results of the simulations are divided by the number of initial histories and by the surface of the scoring bin ($\pi(\rho_{>}^2 - \rho_{<}^2)$), which has $\Delta\rho = \rho_{>} - \rho_{<} = 0.1$ mm. The shadow region indicates the semi-aperture of the final collimators of the helmets.

The general trend is similar for the four helmets. The distribution appears to be uniform inside the characteristic aperture, reducing considerably for larger values of ρ . In case of the 14, 8 and 4 mm helmets, a second step at $\rho \sim 6$ mm is observed. This is due to the output collimator of the central body of the collimation system and corresponds, in fact, to the semi-aperture of the beam at the same z , if the helmets were not present. The dashed line in figure 7 indicates this semi-aperture. This step is not observed in the case of the 18 mm

helmet because it is hidden in the sharp reduction of the distribution. Electrons show a similar behaviour.

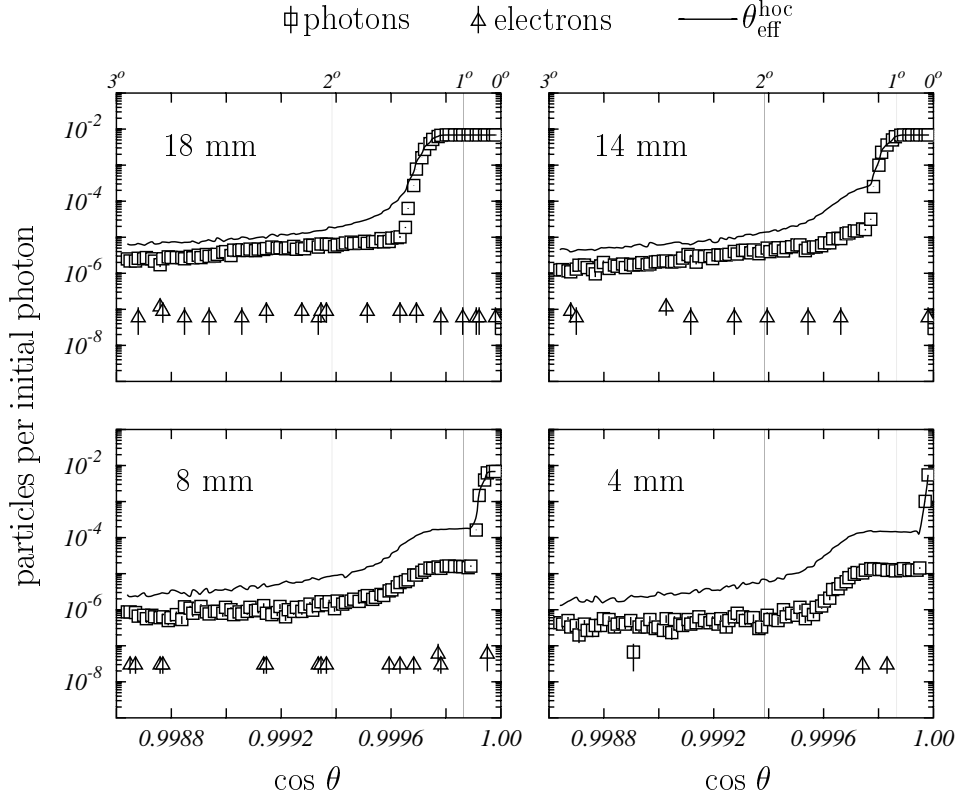


Figure 8. Distributions of particles per initial photon vs. $\cos \theta$ for the trajectories traversing the output collimators of the four treatment helmets. Squares (triangles) correspond to photons (electrons). Solid lines represent distributions of particles per initial photons vs. the effective angle distributions at the same surfaces, $\theta_{\text{eff}}^{\text{hoc}}$.

The particle distribution vs. the angle θ of the particle trajectories once they pass through the helmet output collimators deserves also to be analysed. Figure 8 shows with squares (triangles) the distributions, per initial photon, corresponding to photons (electrons). As we can see, in the case of photons, there is a first region, for angles $\theta \sim 0^\circ$, where the distribution is uniform. In the case of the two smallest helmets, a second region of uniformity appears for larger angles. The first one is related to the characteristic aperture of each helmet collimator, while the second is linked to the aperture of the final collimator of the central body.

In the figure we have also plotted (full curves) the distributions of the fraction of initial photons vs. the cosine of the effective emission angle determined at the helmet outer collimators, $\theta_{\text{eff}}^{\text{hoc}}$. These distributions are very similar to the previous ones, the main difference being that those corresponding to the output angles show a larger reduction after the first region of uniformity. This points out the strong angular focalization produced by the collimation system.

In what refers to the electron distributions, they show very low statistics what indicates that their contribution to the dosimetry of the GK is not relevant.

3.4. Correlations

An important aspect concerning the characteristics of the beams is that associated to the correlations between the relevant variables, these are, the energy of the particles, their positions and the angles defining their trajectories once they reach the output helmet collimators.

The study of the correlations of the energy with ρ and θ shows that, as expected from the previous results, particles with energies other than the initial one are practically not present, irrespective of the ρ or θ values one considers.

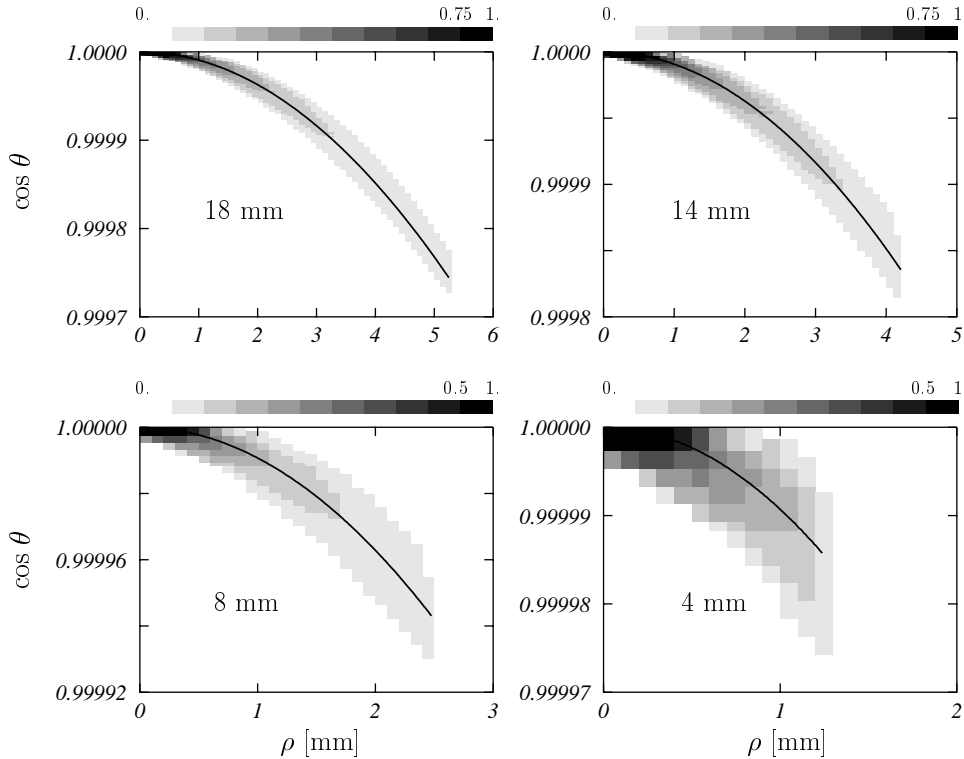


Figure 9. Correlations between the ρ distance to the beam centre and $\cos \theta$ for the particle trajectories at the output collimators of the four treatment helmets. Solid lines represent the curves corresponding to the mathematical collimation considered in the simplification described in the text.

A more interesting result is shown by the correlations between the geometrical variables. Figure 9 shows the results found for ρ and $\cos \theta$ and, as we can see, there exists a strong correlation between both variables: the angle where the $\cos \theta$ distribution is peaked increases with ρ . In this respect it is worth to note that we have used a non-linear gray scale in order to enhance the regions with lower correlations. These results agree with the findings of Moskvin *et al* (2002).

However, these are not the unique correlations between the geometrical variables involved in the problem. Figure 10 represents the correlations shown by the azimuthal angle of the trajectory of the particle and the quantity $\tan^{-1}(y/x)$ calculated with the coordinates of this trajectory at the output helmet collimators. As we can see, these two quantities are strongly correlated for the four treatment helmets. The larger spread shown by the helmets

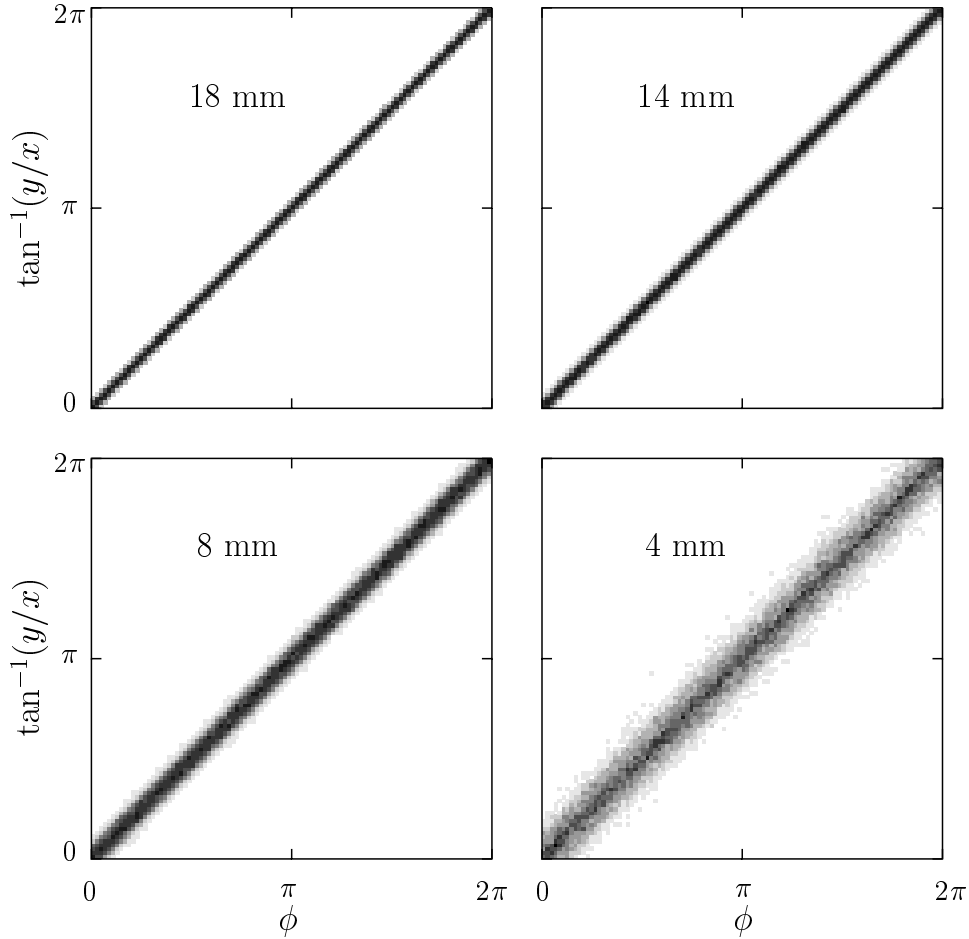


Figure 10. Correlations between the azimuthal angle ϕ and $\tan^{-1}(y/x)$ for the particle trajectories at the output collimators of the four treatment helmets.

with the smaller collimators are due to the lower statistics in these cases. This correlation was not explicitly mentioned by Moskvin *et al* (2002), but, however, it is on the basis of the simplification of the source channel geometry we discuss below.

To test these correlations we have found, we have performed a new simulation in which the particles are emitted from the helmet outer collimators, according to the distributions discussed above and conditioned to these correlations. The procedure we have carried out has been the following. First, we have sampled the initial position (x, y) uniformly within the aperture of the helmet outer collimators. Second, the value of $\cos\theta$ for the trajectory has been sampled according to the conditional distribution for the corresponding ρ value (see figure 9). Finally, the azimuthal angle ϕ has been sampled according to the conditional distribution corresponding to the particular value $\tan^{-1}(y/x)$ (see figure 10). Only photons with initial energy fixed to the maximum value 1.25 MeV have been considered and a total of $2 \cdot 10^7$ histories has been followed. This strategy coincides with that used by Moskvin *et al* (2002). The results obtained in this way (solid lines) are compared to those obtained with the full GK geometry (open circles) in figure 11, normalized to the maximum. As we can see, the agreement between both calculations is rather satisfactory.

In order to understand the implications of the correlations we have encountered in the

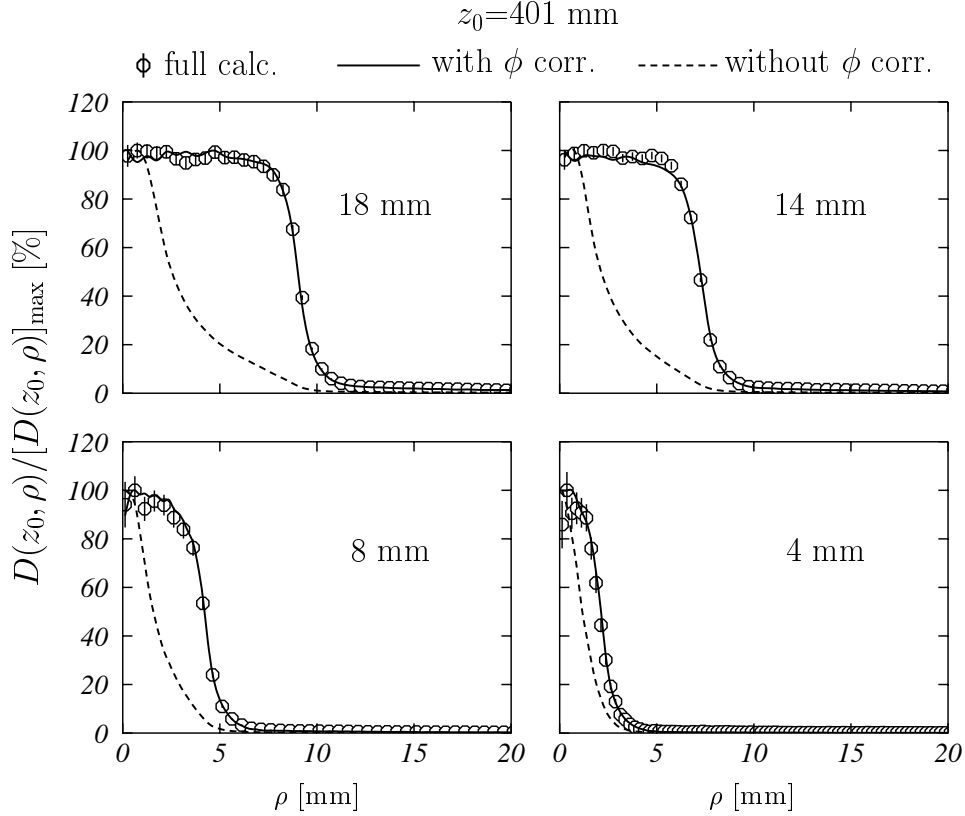


Figure 11. Dose profiles (relative to their maximum) as a function of the radial distance from the beam axis ρ . The results obtained in our simulations at the plane $z_0 = 401$ mm for the four helmets are shown. Open circles correspond to our full calculation. Solid lines have been obtained by taking into account the correlations found for the different variables (see text). Dashed lines correspond to a similar calculation but ignoring the ϕ angle correlations, that is by sampling the ϕ angle uniformly between 0 and 2π .

dosimetry of the GK, we have performed a new simulation following the same procedure, but neglecting the correlations shown by the azimuthal angle ϕ , which has been sampled uniformly between 0 and 2π . The results obtained are shown, again normalized to the maximum, with dashed lines in figure 11. As we can see, if the ϕ angle correlations are neglected, the shape of the dose profile at the focus is strongly modified, showing a big enhancement at distances close to the beam axis.

3.5. Simplification of the source

The simplification in the description of the source of the GK that we propose in this work consists in substituting the full source channel by a “mathematical collimator” in which a point source situated in the center of the active core, emits photons with initial energy equals to 1.25 MeV in the cone defined by itself and the outer collimators of the treatment helmets.

The reasons for that rely, first, on the characteristics distributions (energy, position and polar angle) of the particles traversing the collimation channel, and, second and mainly, on the strong correlations shown by ϕ and $\tan^{-1}(y/x)$ and by θ and ρ , respectively. In fact, if we

assume the simplification mentioned, it is obvious that the azimuthal angle ϕ of a trajectory is related to the point (x, y) at which it reaches the outer collimator source as (see the scheme in figure 1c)

$$\phi \equiv \tan^{-1}(y/x),$$

a value which is in agreement with the maximum of the distributions in figure 10. On the other hand, in this simplified situation, the polar angle θ of this trajectory is related to the corresponding value of ρ in this surface as

$$\tan \theta \equiv \frac{\rho}{z_{\text{col}}},$$

where z_{col} is the z coordinate of the output collimator of the helmets (236 mm in our case). In figure 9 we have plotted, with solid lines, the quantity $\cos[\tan^{-1}(\rho/z_{\text{col}})]$ and, as we can see, it fits perfectly the maximum of the respective distributions.

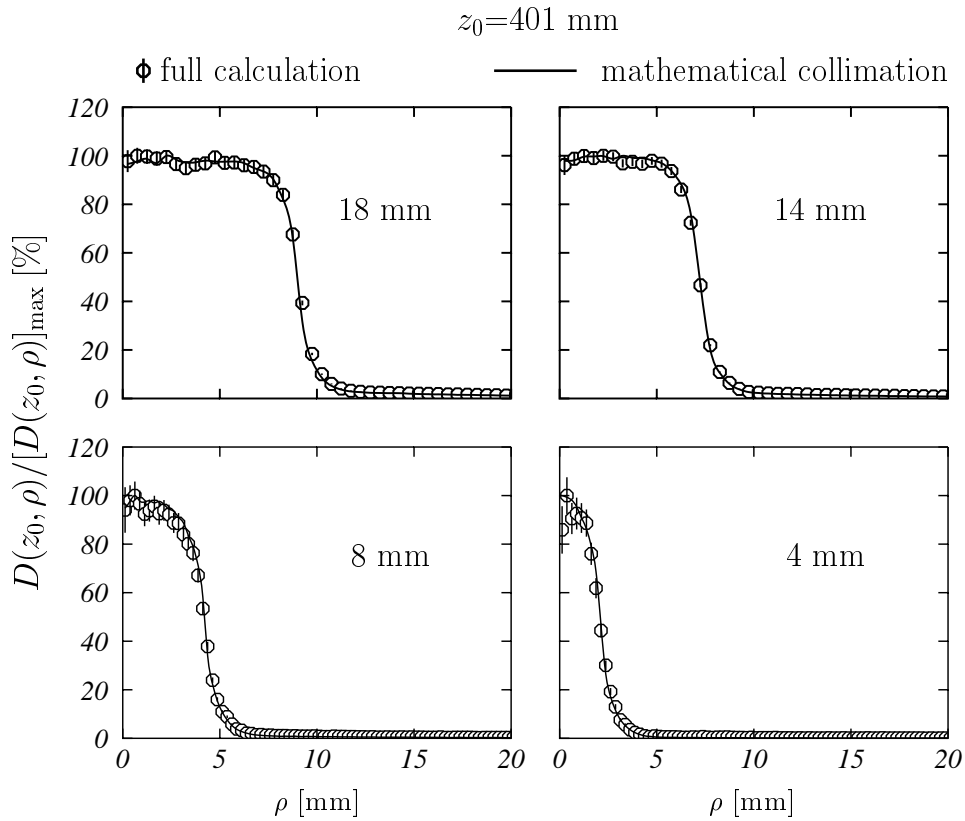


Figure 12. Dose profiles (relative to their maximum) as a function of the radial distance from the beam axis ρ . The results obtained in our simulations at the plane $z_0 = 401$ mm for the four helmets are shown. Open circles correspond to our full calculation. Solid lines represent the calculation done with the simplified model we have proposed.

In order to check the goodness of this simplification, we have performed a new simulation following $2 \cdot 10^7$ histories, assuming a point source situated at the center of the ^{60}Co source, considering only photons with initial energy 1.25 MeV and performing a “mathematical collimation” by sampling the initial particle directions isotropically inside the corresponding

cones with apertures equal to the diameters of the helmet outer collimators given in table 1. The results, normalized to the maximum, are plotted with solid lines in figure 12, where we compare them with those of the simulation considering the full GK geometry (open circles). The uncertainties in the case of the simplified model are a factor 3 (at least) smaller than those quoted for the full GK geometry. The agreement between both simulations is remarkable. In the region of maximal dose, the relative differences between both calculations are within 3%, for the 18 and 14 mm helmets, and 10%, for the 8 and 4 mm ones, where the uncertainties of the full calculation results are relatively large. This shows the feasibility of this simplification.

Besides, this simplified model provides a large reduction (more than a factor 15) in the CPU time needed to perform the simulations.

4. Conclusions

In this work we have investigated the dosimetry of a single-source configuration of the Leksell GammaKnife[®] using the Monte Carlo code PENELOPE (v. 2001). To do that a series of simulations have been performed from which the following conclusions can be drawn:

- (i) We have found that a maximum angle $\theta_{\max} = 3^\circ$ for sampling the initial direction of the emitted photons is enough to ensure the accuracy of the results.
- (ii) The characteristics of the beam after it goes through the output collimators of the helmets indicate that most of the particles traversing these collimators are photons coming directly from the ^{60}Co source.
- (iii) The polar angle θ and the distance to the beam axis ρ of the particle trajectories at the output collimators of the helmets are strongly correlated. The same happens for the azimuthal angle ϕ and the ratio y/x of the corresponding coordinates.
- (iv) These strong correlations can be explained by assuming that the collimation system acts as a mathematical collimator in which the particles are emitted in a cone defined by the output collimators of the helmets and come from a point source located at the center of the active core.

The results obtained with the simplified geometry model we propose here are in good agreement with those found for the full geometry. Besides, the CPU time needed to perform the simulations is largely reduced. This opens the possibility to use MC tools for planning purposes in the GK. Obviously, a comparison of the results obtained from calculations based on this simplified approach, for various configurations of the 201 sources of the GK, with previous works is necessary. Also it is worth to perform a detailed analysis of the corresponding output factors. Work in these directions is being done and will be published in a forthcoming paper.

Acknowledgments

Authors wish to acknowledge G. Rey for useful discussion and for providing us with geometrical details of the Leksell GammaKnife[®]. F.M.O. A.-D. acknowledges the A.E.C.I. (Spain) and the University of Granada for funding his research stay in Granada (Spain). This work has been supported in part by the Junta de Andalucía (FQM0225).

References

- Benjamin W C, Curran W J Jr., Shrieve D C and Loeffler J S 1997 Stereotactic radiosurgery and radiotherapy: new developments and new directions. *Semin. Oncol.* **24** 707-14
- Cheung J Y C, Yu K N, Ho R T K and Yu C P 1999a Monte Carlo calculations and GafChromic film measurements for plugged collimator helmets of Leksell GammaKnife unit *Med. Phys.* **26** 1252-6
- Cheung J Y C, Yu K N, Ho R T K and Yu C P 1999b Monte Carlo calculated output factors of a Leksell GammaKnife unit *Phys. Med. Biol.* **44** N247-9
- Cheung J Y C, Yu K N, Ho R T K and Yu C P 2000 Stereotactic dose planning system used in Leksell GammaKnife model-B: EGS4 Monte Carlo versus GafChromic films MD-55 *Appl. Radiat. Isot.* **53** 427-30
- Cheung J Y C, Yu K N, Yu C P and Ho R T K 1998 Monte Carlo calculation of single-beam dose profiles used in a gamma knife treatment planning system *Med. Phys.* **25** 1673-5
- Cheung J Y C, Yu K N, Yu C P and Ho R T K 2001 Dose distributions at extreme irradiation depths of gamma knife radiosurgery: EGS4 Monte Carlo calculations *Appl. Radiat. Isot.* **54** 461-5
- Elekta 1992 *Leksell Gamma Unit-User's Manual* (Stockholm: Elekta Instruments AB)
- Elekta 1996 *Leksell GammaPlan Instructions for Use for Version 4.0-Target Series* (Geneva: Elekta)
- Hartmann G H, Lutz W, Arndt J, Ermakov I, Podgorsak E B, Schad L, Serago C and Vatinisky S M (ed) 1995 Quality assurance program on stereotactic radiosurgery *Report from a Quality Assurance Task Group* (Berlin: Springer)
- Moskvin V, DesRosiers C, Papiez L, Timmerman R, Randall M and DesRosiers P 2002 Monte Carlo simulation of the Leksell GammaKnife: I. Source modelling and calculations in homogeneous media *Phys. Med. Biol.* **47** 1995-2011
- Salvat F, Fernández-Varea J M, Acosta E and Sempau J 2001 *PENELOPE, a code system for Monte Carlo simulation of electron and photon transport* (Paris: NEA-OECD)
- Semapu J, Sánchez-Reyes A, Salvat F, Oulad ben Tahar H, Jiang S B and Fernández-Varea J M 2001 Monte Carlo simulation of electron beams from an accelerator head using PENELOPE *Phys. Med. Biol.* **46** 1163-86
- Solberg T D, DeMarco J J, Holly F E, Smathers J B and DeSalles A A F 1998 Monte Carlo treatment planning for stereotactic radiosurgery *Radiother. Oncol.* **49** 73-84
- Wu A 1992 Physics and dosimetry of the gamma knife *Neurosurg. Clin. N. Am.* **3** 35-50
- Wu A, Lindner G, Maitz A, Kalend A, Lunsford L D, Flickinger J C and Bloomer W D 1990 Physics of gamma knife approach on convergent beams in stereotactic radiosurgery *Int. J. Radiation Oncology Biol. Phys.* **18**, 941-9
- Xiaowei L and Chunxiang Z 1999 Simulation of dose distribution irradiation by the Leksell Gamma Unit *Phys. Med. Biol.* **44** 441-5